Body Topography Parcellates Human Sensory and Motor Cortex

Esther Kuehn[1,2,3,4], Juliane Dinse[5,6,†], Estrid Jakobsen[7], Xiangyu Long[1], Andreas Schäfer[5], Pierre-Louis Bazin[1,5], Arno Villringer[1], Martin I. Sereno[2] and Daniel S. Margulies[7]

[1]Department of Neurology, Max Planck Institute for Human Cognitive and Brain Sciences, Leipzig 04103, Germany, [2]Department of Psychology and Language Sciences, University College London, London WC1H 0DG, UK, [3]Center for Behavioral Brain Sciences Magdeburg, Magdeburg 39106, Germany, [4]Aging and Cognition Research Group, DZNE, Magdeburg 39106, Germany, [5]Department of Neurophysics, Max Planck Institute for Human Cognitive and Brain Sciences, Leipzig 04103, Germany, [6]Faculty of Computer Science, Otto-von-Guericke University, Magdeburg 39106, Germany and [7]Max Planck Research Group for Neuroanatomy & Connectivity, Max Planck Institute for Human Cognitive and Brain Sciences, Leipzig 04103, Germany

Address correspondence to Esther Kuehn, Department of Neurology, Max Planck Institute for Human Cognitive and Brain Sciences, Leipzig 04103, Germany. Email: ekuehn@cbs.mpg.de

[†]Co-first author.

Abstract

The cytoarchitectonic map as proposed by Brodmann currently dominates models of human sensorimotor cortical structure, function, and plasticity. According to this model, primary motor cortex, area 4, and primary somatosensory cortex, area 3b, are homogenous areas, with the major division lying between the two. Accumulating empirical and theoretical evidence, however, has begun to question the validity of the Brodmann map for various cortical areas. Here, we combined in vivo cortical myelin mapping with functional connectivity analyses and topographic mapping techniques to reassess the validity of the Brodmann map in human primary sensorimotor cortex. We provide empirical evidence that area 4 and area 3b are not homogenous, but are subdivided into distinct cortical fields, each representing a major body part (the hand and the face). Myelin reductions at the hand–face borders are cortical layer-specific, and coincide with intrinsic functional connectivity borders as defined using large-scale resting state analyses. Our data extend the Brodmann model in human sensorimotor cortex and suggest that body parts are an important organizing principle, similar to the distinction between sensory and motor processing.

Key words: embodiment, hand–face border, parcellation, plasticity, septa

Introduction

The division within the human central sulcus between somatosensory cortex for sensation and motor cortex for action is perhaps one of the most deep-seated concepts in neuroscience and constitutes a starting point for thinking about structure, connectivity, function, and plasticity.

Early neuroanatomists such as Flechsig (1920) suggested a modification of this model. Flechsig's (1920) extensive postmortem

studies of cortical myelination identified separable segments within somatosensory cortex area 3b and motor cortex area 4 that he related to specific representations of the body. Because these segments were separated by sharp borders and orthogonal to the classical anterior–posterior division of sensorimotor cortex, Flechsig separated area 3b and area 4 into multiple subfields—in contrast to Brodmann (1909), who suggested that both areas were homogenous. Whereas the Brodmann atlas has since received widespread attention and constitutes a starting point for understanding the sensorimotor system, Flechsig's topographic parcellation model has remained largely overlooked to this day.

Here, we investigated the hypothesis that the human sensorimotor cortex is ordered according to a topographic parcellation scheme as originally suggested by Flechsig. We applied recent advances in in-vivo human brain parcellation (Glasser and Van Essen 2011; Sereno et al. 2013; Lutti et al. 2014; Stüber et al. 2014; Dinse et al. 2015; Tardif et al. 2015), and combined them with functional topographic maps, and intrinsic signal fluctuations as obtained during the resting state (Biswal et al. 1995; Smith et al. 2009) to investigate the relationship between cortical myeloarchitectonic variations, topographic field boundaries between hand and face representations in area 3b and area 4, and intrinsic cortical activity in vivo.

We demonstrate that major myeloarchitectonic borders exist not only between area 3b and area 4 (i.e., between sensory and motor cortices), but also between the representations of the hand and the face in both of these areas, essentially dividing them into (at least) 4 distinct cortical fields. The robustness of our finding across areas (area 3b and area 4), imaging modalities (T_1-based and T_2^*-based), field strengths (3 T and 7 T), myelin mapping techniques (ratio-based and quantitative), physiological parameters (activation and connectivity patterns), and data sets (large-cohort data $N > 400$, individual data sets), as well as the cortical layer-specificity of the myelin reductions show that cortical microstructure varies at boundaries between body parts just as prominently as it does between sensory and motor cortices—confirming the basic assumptions of a topographic parcellation model in humans.

Materials and Methods

Large-Scale Analyses

Participants
To investigate the relation between topographic maps and cortical myelination during active motor movements and during rest, we first used cortical myelin maps and functional imaging data as provided by the Human Connectome Project (HCP, see below for single subject data acquired at 7 T). Myelin maps and hand/face functional activity data were available for $N = 440$ participants. All participants were healthy and none of them suffered any psychiatric or neurological disorder. All data are provided open-source (http://www.humanconnectome.org/documentation/S500).

MRI Data Acquisition
Structural HCP data were acquired with a 32-channel head coil on a 3 T Siemens Skyra. Two 0.7-mm isotropic T_1-weighted (T1w) MPRAGE scans (256 slices, sagittal orientation, AP phase encoding direction, field of view [FOV] read: 224 mm, FOV phase: 100%, time repetition [TR] = 2400 ms, time echo [TE] = 2.14 ms, time to inversion [TI] = 1000 ms, and flip angle [FA] = 8°) and two 0.7 mm isotropic T2w scans (same FOV and slices as in the T1w

scan, TR = 3200 ms, and TE = 565 ms) were used per subject (Glasser et al. 2013). In the T2w images, TE was lengthened to improve intracortical contrast for myelin detection (Glasser et al. 2013). As part of the HCP pipeline, only structural scans rated as "good" or "excellent" are released (Van Essen et al. 2013).

Functional Data Acquisition
Functional HCP data were acquired with a 32-channel head coil on a 3 T Siemens Skyra. Whole-brain EPI data had an isotropic voxel resolution of 2 mm. A relatively small TR of 720 ms was used to increase the sensitivity to detect resting state signal fluctuations (Smith, Beckmann, et al. 2013). The imaging parameters were TE = 33.1 ms, FA = 52°, and FOV = 208 × 180 mm. Of note, 72 slices were acquired using a multiband acceleration factor of 8. Four 15-min resting state fMRI runs per subject were acquired in 2 separate sessions. In the first session, 15-min right-to-left phase encoding was followed by 15-min left-to-right phase encoding; in the second session, the order was reversed. Interleaved slice-acquisition was applied. In addition, a single-band reference image was acquired at the beginning (FOV read direction = 180 mm, FOV phase encoding direction = 180 mm, FOV inferior–superior direction = 144 mm, 72 slices, and interleaved slice ordering).

Task Description
During the resting state scans, participants were lying in the scanner with eyes open. They were asked to think about nothing in particular and not to fall asleep. After 2 resting state scans (15 min each), participants proceeded with task-based imaging experiments. For our analyses, we used the resting state scans of 2 imaging sessions, that is, four 15-min scans.

During the functional mapping paradigm, participants were presented with randomized written instructions that indicated to them which movement to execute (i.e., "Hand," "Foot," and "Tongue"). Instructions were presented for 3 s. After this, movement execution started and continued for 12 s. Participants were presented with a fixation cross during movement execution. Fifteen-second rest conditions separated successive blocks. The experiment was tested in 2 runs, with 2 tongue movements and 4 hand movements (2 left and 2 right), and 4 foot movements (2 left and 2 right) per run (Yeo et al. 2011). The tongue movements activated lip, lower face, and tongue representations. Lip and lower face representations are superior to tongue representations (Zeharia et al. 2015) and border thumb representations (Jain et al. 1997; Manger et al. 1997; Nakamura et al. 1998).

Cortical Surface Extraction and Normalization
The HCP structural MRI processing pipeline includes image distortion correction (Jovicich et al. 2006) and averaging the 2 acquired scans. Cortical segmentation was performed using FreeSurfer. For cortical folding-based intersubject registration to a group-average surface template, a multimodal surface matching algorithm (Smith, Beckmann, et al. 2013; Robinson et al. 2014) was applied in unimodal (sulcal depth only) mode. A B1 (bias field) correction was performed and the data were transformed nonlinearly into MNI space. Cortical myelin maps were extracted from structural images by computing the ratio of the T1w and T2w image values at each voxel between the white and pial surfaces, and mapping this ratio to the cortical surface (Glasser and Van Essen 2011; Glasser et al. 2013). The HCP myelin maps used in the present study were chosen

because they are improved over those available in previous HCP data releases (Glasser et al. 2013).

Preprocessing of Functional Data (Functional Mapping)

We used preprocessed images offered by the HCP pipeline (Glasser et al. 2013; Smith, Monaghan, et al. 2013). FSL and FreeSurfer software packages were used to perform gradient unwarping, motion correction, fieldmap-based EPI distortion correction, brain-boundary-based registration of EPI data to structural T1w scan, nonlinear (FNIRT) registration into MNI space, and grand-mean intensity normalization. The data were smoothed using an unconstrained 3D Gaussian kernel of FWHM = 4 mm. Activity estimates were computed using the general linear model (GLM) as implemented in FSL's FMRIB's Improved Linear Model (FILM) with autocorrelation correction (Woolrich et al. 2001). Predictors were convolved with a double gamma "canonical" hemodynamic response function (Glover 1999) to generate the main model regressors. Five predictors covered the 12-s blocks: "right-hand movement," "left-hand movement," "right foot movement," "left foot movement," and "tongue." One predictor covered the cue period prior to each motor block (3 s). Temporal derivative terms derived from each predictor were added to each GLM and were treated as confounds of no interest. The functional data were filtered with a Gaussian-weighted linear high-pass filter with a cutoff of 200 s. The time series was prewhitened within FILM to correct for autocorrelations in the fMRI data. Surface-based autocorrelation estimate smoothing was incorporated into FSL's FILM at a sigma of 5 mm.

Preprocessing Functional Data (Resting State)

The preprocessing is in detail described elsewhere (Glasser et al. 2013; Smith, Beckmann, et al. 2013). Briefly, the functional data were corrected for spatial distortions caused by gradient nonlinearity and were corrected for head motion by registering the time series to the single-band reference image. In order to distortion correct the EPI images, the 6 spin-echo images were fed into FSL's "Topup" to estimate a single fieldmap image (Glasser et al. 2013). The data were registered to the T1w structural image by using the single-band reference image as the representative fMRI image during alignment (Glasser et al. 2013). The data were concatenated, together with the structural-to-MNI nonlinear warp field, and this single resulting warp (per time point) was applied to the original time series to achieve a single resampling into 2-mm MNI space. Global intensity normalization was applied and nonbrain voxels were masked out. A minimal low-pass filter with a cutoff of 2 s was applied. To remove artifacts, an independent component analysis using MELODIC with automatic dimensionality estimation, limited to a maximum of 250, was applied. These components were fed into FIX, which classifies components into "good" versus "bad." Bad components were then removed from the data. Functional data were mean gray-matter time series regressed.

Data were mapped onto the native cortical surface. Time series were resampled from the original FreeSurfer surface onto a lower resolution registered standard mesh of 2-mm average vertex spacing and regularized with 2-mm FWHM surface smoothing. The same artifactual processes as described above were then removed from the grayordinate version of the data by first applying the same high-pass temporal filtering and then regressing the bad component's time series out. The resulting runs were combined across subjects using variance normalization of the time series (using the same approach as MELODIC, Beckmann and Smith 2004).

Statistical Analyses

As part of the HCP pipeline, fixed-effect analyses were conducted using FSL's FMRI Expert Analysis Tool (FEAT) to estimate the average effects across runs within-subjects. Linear contrasts were computed at the first level to estimate activation for each movement type versus all other movement types. Mixed-effect analyses treating subjects as random effects were conducted using FSL's FMRIB's Local Analysis of Mixed Effects (FLAME) to estimate the average effects of interest for the group using one-sample t-tests. Statistical analyses were conducted separately for the left and right hemispheres, and surface outputs were combined at the conclusion of analysis.

To identify hand and face representations, we used an adaptive thresholding algorithm. We first identified the peak of each cluster and started thresholding at the lowest z-value within each area. We stepwise reduced cluster size until a predefined cluster size of 400 vertices was reached (Long et al. 2014). The z-threshold was set at $z > 5$. The extension of the cluster was restricted by the left-hemispheric FreeSurfer surface labels of area 3b and area 4. We sampled z-values of hand and face task activation maps between the hand and face representations by sampling superior to inferior parallel to the central sulcus. We sampled z-values along the path, and calculated the intersection points between hand and face task activation maps to functionally define the hand–face border.

We sampled group-averaged as well as individual cortical myelin content within and between hand and face representations using the cortical paths as specified above. The peak detection algorithm was used to calculate global and local minima and maxima, and maximal slope differences were used to detect local turning points. We correlated the T1w/T2w ratios sampled between the peaks and the global minimum within the hand and face representations with the z-values obtained using the contrasts hand – (face + foot), and face – (hand + foot), respectively, using Spearman rank coefficients. We used a corrected P-value of $P < 0.0125$ to identify significant correlations. T1w/T2w ratios of the above specified cortical paths were extracted of individual participants and compared with neighboring values ($P < 0.0025$, Bonferroni-corrected).

As part of the HCP processing pipeline, a group-PCA (principal component analysis) was applied on the combined time series that approximates full temporal concatenation of all subjects' data, outputting the strongest 4500 spatial eigenvectors (PCA components, weighted by the eigenvalues). We created a spatial correlation matrix for each vertex by correlating each row within the spatial eigenvector map with each other row using Pearson correlations. The Fisher z-transformed r-value of each vertex thus represented the similarity of the functional connectivity profile of this vertex to all other vertices. The "max statistic" method was used for adjusting the P-values of each correlation for multiple comparisons (Groppe et al. 2011a, 2011b). Like Bonferroni correction, this method adjusts P-values in a way that controls for the familywise error rate. A significance threshold of $P < 0.05$ was applied. To assess local variation in functional connectivity, we calculated the mean correlation of each node with its neighbors within a 4 mm radius (based on exact geodesic distance [Mitchell et al. 1987], as implemented in https://code.google.com/p/geodesic/). Correlation values were Fisher's r-to-z transformed before averaging within a scan. The 4 within-scan maps

were then averaged on the individual-level before group-level analyses.

Individual Participant Analyses Using Quantitative Imaging at 7 T

Participants

In order to validate the large-scale analyses as conducted above on the single subject level with improved spatial resolution and improved imaging processing tools, additional functional and structural data were acquired for 7 healthy human participants (25.6 years ± 3.0 years, 5 females), who participated in 2 MR scanning sessions. None of the participants had a history of any neurological or psychological disorder. Informed consent was given prior to scanning, and all participants were compensated for their attendance. The study was approved by the Ethics committee at the University of Leipzig.

MRI Data Acquisition

Structural ultra-high-resolution MRI data were acquired at a 7 T MAGNETOM Siemens MR scanner situated in Leipzig, Germany. A 24-channel head coil was used. For each participant, quantitative images of the T_1 relaxation time as well as T1w images were obtained by using an MP2RAGE sequence (Marques et al. 2010), and a TR-FOCI pulse for inversion (Hurley et al. 2010). A whole-brain image at 0.7-mm isotropic resolution (TI1/TI2 = 900/2750 ms, TR = 5 s, TE = 2.45 ms, alpha1/alpha2 = 5°/3° and no GRAPPA) and images of the 2 individual hemispheres at 0.5 mm isotropic resolution were acquired (same parameters as above, with GRAPPA = 2 and total scanning time 75 min). One participant (P6) took part in 2 additional scanning sessions, where ultra-high-resolution T_2*-weighted images with a resolution of 0.5 mm isotropic (multi-echo FLASH sequence, TE1–4 = 9.18 ms, 17.33 ms, 25.49 ms, 33.65 ms, TR = 44 ms, GRAPPA = 2, and scan time: 26 min, Tardif et al. 2016), and T_2* and T_1 images at lower resolution were obtained (0.6 and 0.7 mm isotropic, multi-echo T_2* FLASH sequence, TE1-2 = 8.16 ms, 18.35 ms, TR = 29 ms, GRAPPA = 3; T_1 sequence: parameters same as above).

FMRI data were acquired at a 3 T VERIO Siemens MR Scanner situated in Leipzig. A 32-channel head coil was used. Twenty slices were acquired at 2 mm isotropic resolution, with interleaved slice timing (gap: 1 mm), TR = 2 s, TE = 30 ms, FA = 90°, and matrix size: 96 × 96. Functional imaging started with 2 resting state scans (6 min each), followed by one hand/face mapping block (12 min), another resting state block (6 min), and another hand/face mapping block (12 min). A T1w anatomical scan was acquired prior to functional imaging (MPRAGE, resolution: [1.3 × 1.3 × 1.2] mm³, TE = 2.83 ms, and TR = 2300 ms). For the first participant, this anatomical scan was not acquired. A fieldmap was acquired prior to functional data acquisition ([3 × 3 × 4] mm³, 30 slices, TR = 488 ms, TE1-2 = 5.19 ms, 7.65 ms, and FA = 60°).

Task

During the functional mapping blocks, participants were visually instructed to tap their right fingers and thumb (one after the other), to move their right foot and toes, or to move their tongue sideways along the inner side of the lip while keeping the mouth closed, respectively. The latter movement activated lip, lower face, and tongue representations. Lip and lower face representations are superior to tongue representations (Zeharia et al. 2015) and border thumb representations (Jain et al. 1997; Manger et al. 1997; Nakamura et al. 1998). Each movement block lasted for 25 s and was alternated with pause blocks that

lasted 15 s. Each condition was repeated 6 times, adding up to 18 trials per block.

Cortical Surface Extraction

Myelin mapping analyses were performed using the CBS Tools software package, a plug-in for the MIPAV software package (McAuliffe et al. 2001) and the JIST pipeline environment (Lucas et al. 2010). The CBS Tools are freely available for download at http://www.nitrc.org/projects/cbs-tools/. The software package is optimized for processing MP2RAGE sequence data acquired at ultra-high field MRI and operates in a fully automated way (Bazin et al. 2014). In multiple steps, structural data were registered and represented in Cartesian space using a level-set framework (Sethian 1999). The 3 T_1 images acquired per subject were first rigidly coregistered to the standard anatomical MNI reference space (6 degrees of freedom), which was optimized using a cost function of normalized mutual information. The 2 single-hemispheric 0.5 mm T_1 images were fused, and data were resampled to a resolution of 0.4 mm (Bazin et al. 2014; Dinse et al. 2015). Intensity normalization was performed to correct for intensity inhomogeneities (Bazin et al. 2014). Several steps were taken to remove extra-cranial tissue to enhance structures with strong partial voluming and to ensure correct folding pattern (Bazin et al. 2014). The CRUISE algorithm (Han et al. 2004) was used to estimate the white matter/gray matter (wm/gm) boundary and the gray matter/cerebrospinal fluid (gm/csf) boundary. Only left hemispheres were processed.

The recently validated equivolume model (Waehnert et al. 2014, 2016) was used to model the surfaces in reference to individual cortical folding patterns and to specify cortical layers. The cortical sheet of each subject was divided into 21 surfaces perpendicular to which traverses were constructed. Traverses run from the wm/gm boundary to the gm/csf boundary. The cortical sheet was initially divided into 21 surfaces (instead of 4), because the 3 most pial and the 2 deepest layers were excluded to reduce an effect of partial voluming on the results (Tardif et al. 2015). The remaining 16 layers were then averaged into 4 equally spaced layers for further analyses. Quantitative T_1 values of MR images were sampled along the traverses at different cortical depth to derive layer-dependent and across-layer myelin content. Finally, cortical surface inflation was performed on the extracted surfaces (Tosun et al. 2004), and layer-dependent T_1 values were mapped onto these inflated surfaces. Cortical thickness (CT) was calculated by computing the normal vector at the wm/gm boundary surface toward the gm/csf boundary.

We obtained a precise co-alignment between the T_2* and the T_1 images by first co-registering the low-resolution T_2* images to the low-resolution T_1 image acquired within the same scanning session using rigid registration in MIPAV. We then coregistered the low-resolution T_1 image onto the high-resolution T_1 image with rigid registration in MIPAV followed by nonlinear alignment with ANTS (Avants et al. 2008), and performed the same co-registration between the low- and high-resolution T_2* images. Through composition of all transformations with the CBS Tools, we obtained a matching between the high-resolution T_2* and the high-resolution T_1 image with a single interpolation step. Both images being in the same space as the T_1 image allowed us to use the wm/gm and gm/csf surface boundaries as obtained from T_1-based segmentation for T_2*-based analyses.

Functional Data Preprocessing

Functional imaging data were first preprocessed using SPM8 (Statistic Parametric Mapping, Wellcome Department of

Imaging Neuroscience, University College London, London, UK) using standard pipelines and were then coregistered to the structural data using MIPAV. A slice timing correction and realignment were applied to correct for differences in image acquisition time between slices, and to minimize movement artifacts in the time series. Functional data were unwarped and distortion corrected using FSL FMRIB's Utility for Geometrically Unwarping EPIs (FUGUE) using the acquired fieldmap.

For registration, functional imaging data were averaged and corrected for inhomogeneities using a shading correction algorithm (kernel FWHM: 0.15 and Wiener filter noise: 0.01) implemented in MIPAV. Subjectwise registration to the anatomical T1w scan (acquired within the same scanning session as the functional data) was performed using landmark-based least-square registration. Correct registration within sensorimotor areas was visually checked voxel-by-voxel (with functional and anatomical images greatly zoomed in such that individual voxels were clearly visible) and was stepwise improved until a plateau was reached (typically 8–12 iterations). Stepwise improvements included placing manual landmarks at enlarged voxels at corresponding locations within functional and structural images, which informed an automated algorithm to realign the images based on these landmarks. A plateau was reached when no further improvement on the voxel-level could be detected after 3 iterations. An overview about registration accuracy can be inspected in Supplementary Figure 1.

In a second step, the T1w scans acquired at 3 T during fMRI scanning were registered to the 0.7 mm T_1 images acquired at the 7 T scanner using FNIRT (FMRIB's nonlinear image registration tool). In 2 subjects (one subject: no available anatomical 3 T scan, second subject: bad quality of anatomical 3 T scan likely due to head motion), functional data were directly registered to 0.7 mm T_1 7-T anatomies. The use of nonlinear automated registration allowed correcting for scanner-specific distortions. The 0.7 mm 7-T T_1 scans were then linearly registered to the ultra-high-resolution T_1 image (0.4 mm) using FLIRT. These registration matrices were applied to the functional data to register them to the high-resolution structural images. Note that although slightly different registration approaches were used for these 2 subjects due to the lack of a 3-T T1w scan (i.e., down-sampling from 2 mm to 1.2 mm versus down-sampling from 2 mm to 0.7 mm), registration accuracy was high across all subjects (see Supplementary Fig. 1). In addition, FreeSurfer labels of primary somatosensory cortex and primary motor cortex, that is, area 3b and area 4, were registered to the individual subject's high-resolution surface derived from the 0.7 mm T_1 image using a custom-built registration algorithm implemented in FreeSurfer. This allowed restricting surface-based mapping analyses (see below) to our regions of interest, that is, area 3b and area 4.

In a second analysis stream, functional data were normalized and smoothed with a Gaussian kernel of 3 mm. These analyses were conducted only for reporting results in a standard way (MNI coordinates, normalized, voxel resolution of 3 mm isotropic); they were not used for myelin mapping analyses.

Statistical Analyses

Fixed-effect analyses were conducted using SPM8 to estimate the average effects across runs subject by subject. Regressors were created for each movement type (hand, face, and foot), and for the rest condition (the foot regressor was only included in the model to obtain data comparable to the HCP data set, see above). Six motion parameters were included as regressors of no interest. Linear contrasts were computed at the first level to estimate

activation for each movement type versus all other movement types. Linear contrast images and contrast estimates were computed in 3-dimensional space, and were registered to surface space. Functional data were cluster-corrected with a familywise error correction ($P < 0.05$).

Beta images were mapped onto the cortical surface, and masked with area 3b and area 4 FreeSurfer surface labels. Quantitative T_1 values (ms) in different cortical depths, functional activity (t-values), and cortical thickness (CT) values (mm) were sampled along predefined paths between hand and face representations. The paths were guided by highest probability of labels present in the cortical areas.

For group statistics, we correlated t-values and T_1 values sampled along the paths as specified above using Pearson correlations. We used a corrected P-value of 0.0125 (corrected for 4 comparisons performed in each subject). We sampled T_1 values through cortical depths at locations of peak t-values, and at intersection points between hand and face activation maps (if multiple intersection points were present within one area, the most inferior one was chosen by convention). T_1 sampling was restricted to 16 layers. The 3 most pial and the 2 deepest layers were excluded to prevent an effect of partial voluming on the results (Tardif et al. 2015). Data were averaged to "deep layers" (layers 1–4, close to wm/gm boundary), "inner middle layers" (layers 5–8), "outer middle layers" (layers 9–12), and "superficial layers" (layers 13–16, close to gm/csf boundary) (Tardif et al. 2015). To investigate layer-specific effects, ANOVAs were conducted with the factors location (hand, hand–face border, and face), and layer (deep, inner middle, outer middle, and superficial) for area 3b and area 4. Paired-sample t-tests were conducted within each of the 4 layers to examine whether myelin reductions at the hand–face border could be detected in each layer or only in specific layers. The significant threshold was set at $P < 0.05$ (Sereno et al. 2013). We sampled $1/T_2^*$ values from the T_2^* images that were acquired for one participants (P6) across cortical depths. Values were sampled along the 2 predefined paths, one in area 3b and one in area 4, as specified above.

Results

Reduced Cortical Myelin Between Hand and Face Representations

To investigate the relationship between cortical myelin and body part topography in area 3b and area 4, we obtained structural and functional neuroimaging data from a large data set ($N > 400$, HCP). We used the ratio method (T1w/T2w) as a proxy for cortical myelin in vivo. Functional MR images acquired during hand and face movements were used to map hand and face (in particular lower face, lip, and tongue) representations in human area 3b and area 4 (see Table 1). Whole-brain maps showed high cortical myelination (indicated by high T1w/T2w ratios) in primary sensory and motor cortices (see Fig. 1A), as expected based on prior reports (Flechsig 1920; Hopf 1969; Sereno et al. 1995; Glasser and Van Essen 2011; Dick et al. 2012; Nieuwenhuys 2013). However, we also identified a sharp, S-shaped border that separates area 3b and area 4 horizontally into superior and inferior parts (see Fig. 1A). This border corresponded to the functional hand–face border identified using BOLD imaging (see Fig. 1A,B and see Supplementary Fig. 2A,B for right hemisphere). Paired-sample t-tests revealed that the cortical myelin reductions at the functional hand–face border were significant both in area 3b and in area 4 (all $P < 0.001$, see Fig. 1C).

Table 1. BOLD signal change elicited by hand and face (in particular lip and tongue) movements

Contrast	Hand – (face + foot)				Face – (hand + foot)			
P	Area	t-value	MNI x,y,z	k	Area	t-value	MNI x,y,z	k
1	4	25.44	−36, −22, 44	179	4	20.34	−48, −8, 32	129
	3b	24.84	−38, −24, 54	88	3b	21.39	−54, −16, 34	228
2	4	23.33	−38, −20, 52	194	4	20.89	−44, −16, 38	129
	3b	19.19	−38, −22, 52	62	3b	21.45	−56, −12, 32	231
		12.20	−40, −32, 56	21				
		6.79	−54, −12, 42	6				
3	4	26.86	−36, −26, 54	119	4	23.77	−48, −14, 38	153
	3b	27.24	−52, −14, 42	266	3b	27.24	−52, −14, 42	266
4	4	26.29	−30, −24, 56	159	4	15.33	−52, −6, 34	107
	3b	13.22	−38, −22, 52	40	3b	14.73	−56, −8, 36	149
		13.09	−42, −30, 56	36				
5	4	23.43	−32, −20, 42	254	4	26.45	−44, −6, 32	100
						7.65	−22, −28, 56	18
	3b	13.07	−44, −16, 44	8	3b	17.86	−54, −10, 26	85
		12.69	−46, −18, 52	33		6.07	−20, −34, 64	10
		9.21	−58, −8, 24	12				
6	4	34.90	−38, −22, 54	185	4	30.91	−52, −8, 34	100
		6.31	−14, −32, 60	10		8.03	−36, −18, 40	30
	3b	32.98	−38, −22, 52	140	3b	34.87	−54, −12, 40	137
		13.04	−38, −30, 54	45				
		8.02	−30, −36, 58	5				
7	4	26.93	−36, −20, 52	178	4	19.97	−54, −6, 28	84
	3b	23.13	−44, −28, 54	25	3b	22.82	−56, −6, 30	239
		16.88	−42, −18, 50	83				
Group-average HCP	4	29.32	−39, −19, 65	403	4	31.57	−57, −4, 35	548
	3b	28.74	−41, −21, 60	998	3b	31.36	−57, −6, 35	1024

Notes: Shown are normalized, cluster-corrected (FWE, $P < 0.05$, $k > 5$) single subject results ($n = 7$) for the contrasts hand – (face + foot) and face – (hand + foot). Individual participants (P) are labeled with numbers (corresponding to Supplementary Fig. 3E). The last 2 rows show the group-averaged results of the HCP data set ($N = 460$).

We also found a positive correlation between cortical myelination within hand and face representation areas and the z-scores related to the functional activation during motor movements (face area 3b: $P < 0.5 \times 10^{-15}$, $\rho = 0.96$; hand area 3b: $P < 0.5 \times 10^{-5}$, $\rho = 0.98$; face area 4: $P < 0.005$, $\rho = 0.96$; hand area 4: $P < 0.5 \times 10^{-15}$, $\rho = 0.90$, see Fig. 1D).

Myelin Borders Can Be Identified in Individual Participants Using Quantitative Imaging at 7 T

To investigate whether myelin borders can also be identified in individual participants, we conducted similar analyses on individual data sets acquired at a 7 T MR scanner with the following improvements: 1) We avoided structural normalization to prevent registration-related artifacts, 2) we used a different validated marker to describe cortical myelin (quantitative T_1 values, Stüber et al. 2014; Dinse et al. 2015), 3) we used a biologically motivated algorithm to define cortical layers (Waehnert et al. 2014), and 4) we improved the spatial resolution of the data to prevent smoothing-related artifacts within sensory and motor areas. Again, we found highly myelinated primary sensory and motor cortices within each individual participant (see Supplementary Fig. 3A). Critically, we found a patchy myeloarchitecture within area 3b and area 4 (see Figs 2A,C and 3A; Supplementary Figs 3A and 4A). Local reductions in cortical myelin corresponded to the functional hand–face border as described using BOLD imaging in each individual participant ($n = 7$, see Figs 2A,C and 3A, and Supplementary Fig. 4A). This was confirmed by a significant difference between the myelin content within the border area compared with topographic centers ([hand + face]/2-border, in T_1 (ms) compared with a normal distribution with a mean equal to zero: area 3b: -46.70 ± 33.13, $t(15) = -5.64$, $P = 4.71 \times 10^{-5}$, area 4: -206.96 ms ± 117.36 ms (mean $\pm$ SD), $t(15) = -7.05$, $P = 3.91 \times 10^{-6}$, note that negative values indicate a strong myelin difference, because high T_1 values [ms] indicate low myelin, see Fig. 4B). Note that the latter analyses correct for the general decrease in cortical myelination in inferior compared with superior areas.

Cortical myelination (T_1 values, normalized, inverted) and functional activity (t-values, normalized) at the individual level had positive correlation coefficients (24/28 correlations, where 28 reflected 2 cortical areas [area 3b, area 4] $\times$ 2 representations [hand, face] $\times$ 7 participants), indicating that higher cortical myelination corresponded with higher functional activity within the same area; for 5/7 participants, these correlations reached significance for either area 3b, area 4, or both (see Figs 2B,D and 3B, and Supplementary Fig. 4B). Note that these correlations were not performed to test our hypotheses about a structural myelin border between hand and face areas; a structural hand–face border could well exist also without significant correlations between cortical myelin and BOLD signal change within each topographic area. Those analyses were conducted to provide additional information to the reader on the relationship between cortical myelination and BOLD signal change within topographic areas that may be used as an inspiration for future studies. The results of these correlations will not be part of the discussion.

T_2^*-based image contrast can also be used for in vivo histology of cortical myelin and iron (Deistung et al. 2013; Stüber et al. 2014).
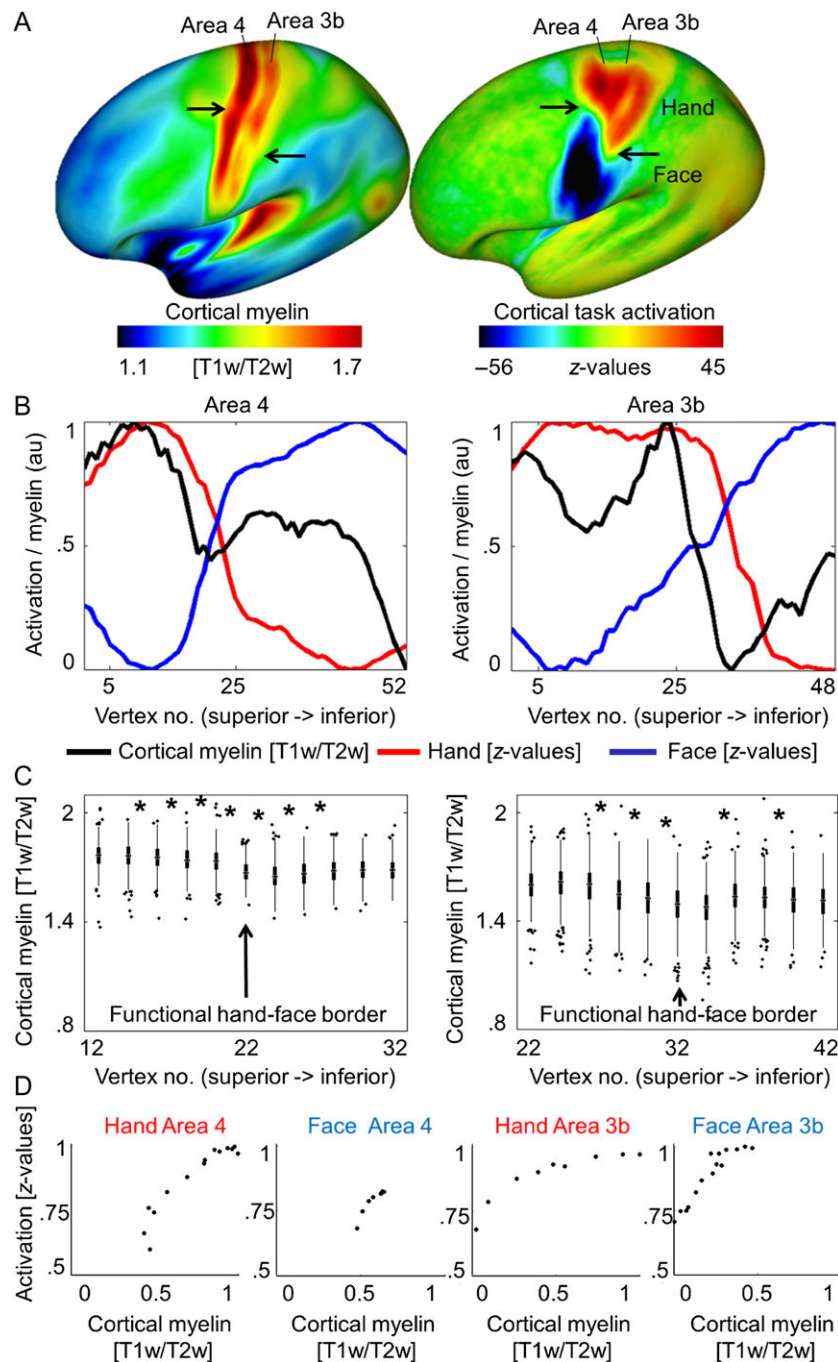
Figure 1. Relationship between cortical myelination and cortical task activation in large-cohort data set (HCP). (A) Cortical myelin content (T1w/T2w) and BOLD signal change (z-values, contrast: hand − [face + foot], face − [hand + foot]) averaged over a large group sample. Arrows indicate the S-shaped border separating hand and face representation areas (see Supplementary Fig. 2 for right hemispheric data). (B) Cortical myelin content (T1w/T2w) and BOLD signal change (z-values) sampled vertically from the superior border of the hand representation to the inferior border of the face representation, parallel to the central sulcus (see Supplementary Fig. 2 for sample paths). Values are normalized to 0–1 using arbitrary units (au). Supplementary Figure 2 shows corresponding right hemispheric plots. (C) Means of individual participants' myelin content (T1w/T2w). Vertex numbers correspond to those in B, values are sampled from the hand–face intersection point ±10 vertices (values sampled from every second vertex, see Supplementary Fig. 2). Edges show 25th and 75th percentiles, whiskers extend to the most extreme data points not considered outliers, outliers are plotted individually. Significant pairwise comparisons (Bonferroni-corrected $P < 0.0025$) are marked with a star. (D) Correlations between cortical myelin content (T1w/T2w) and BOLD signal change (z-values) elicited by hand and face movements within the hand and face representations of area 3b and area 4. Values are sampled along cortical paths (see Supplementary Fig. 2), and normalized to values between 0 and 1 using arbitrary units (au). All 4 correlations reached significance ($P < 0.005$).

For one participant (P6), we investigated whether cortical myelin reductions between hand and face representation areas were visible in T_2^*-based image contrasts. An increase in T_2^* values (depicted as a decrease in $1/T_2^*$ values, indicating a decrease in cortical myelin, see Supplementary Fig. 5) between hand and face representations was present, both in area 3b and in area 4. The effect size was approximately 10% of the total cortical T_2^* signal variation.
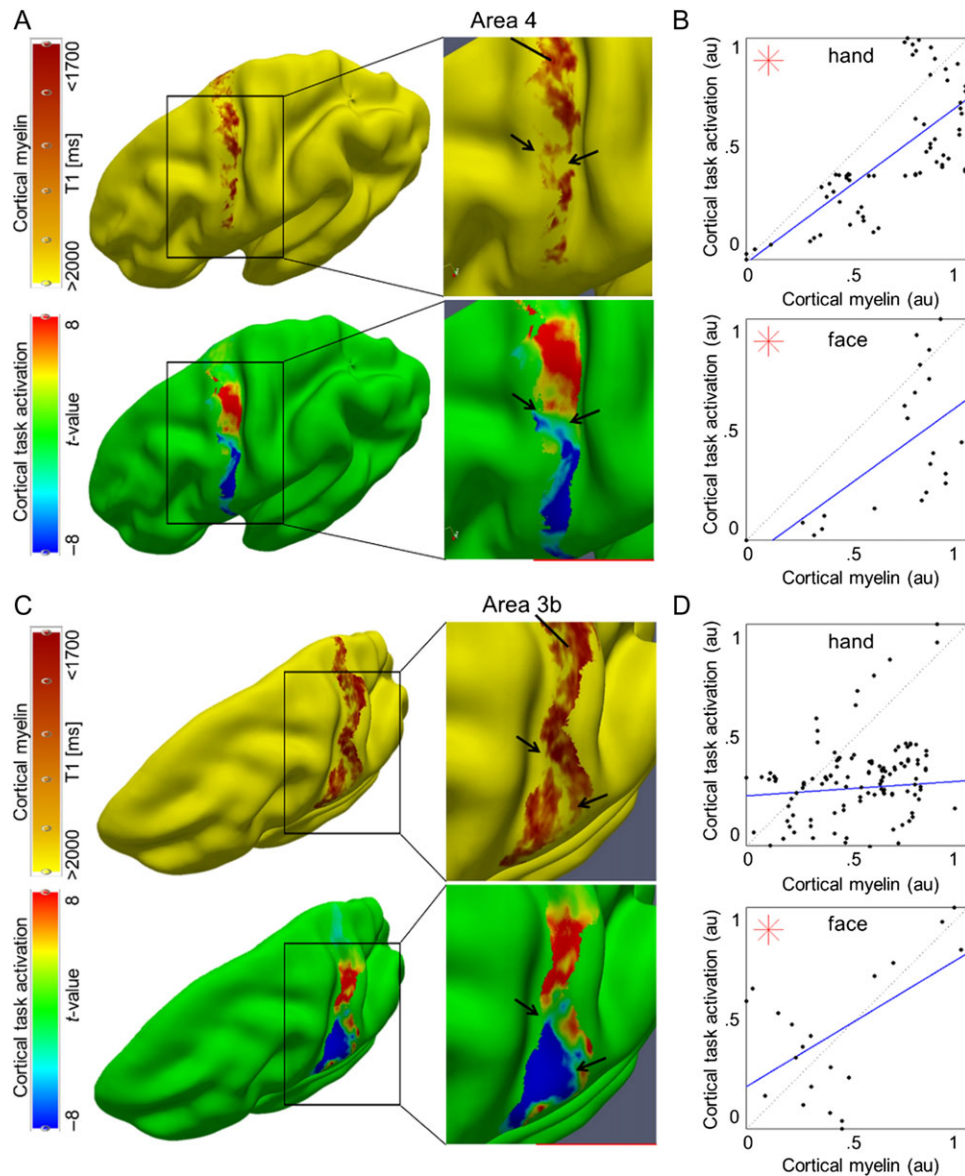
Figure 2. Relationship between cortical myelination and cortical task activation: (*A, C*) Cortical myelin content (T_1 [ms], sampled at 25% cortical depth in A and at 50% cortical depth in (*C*) due to cortical depth-dependent myelin reductions, see Fig. 4) and BOLD signal change (*t*-values) within somatosensory cortex (area 3b) and primary motor cortex (area 4) elicited by hand and face (in particular tongue and lip) movements, respectively, of one individual participant (see Fig. 3 and Supplementary Fig. 4 for remaining participants). The contrast hand – (face + foot) is displayed in red color, the contrast face – (hand + foot) is displayed in blue color. Structural and functional data are masked with FreeSurfer surface labels of area 4 and area 3b, respectively. Two millimeter tangential smoothing (i.e., within cortical layers) was applied to T_1 values for visualization purposes only. (*B, D*) Correlations between cortical myelin content (T_1 values, normalized to [0 1], and inverted to correspond to high myelin) and BOLD signal change (*t*-values, normalized) sampled vertically from hand to face representations within area 4 and area 3b, respectively (see Supplementary Fig. 6C for sampling paths). Significant correlations ($P < 0.0125$) are marked with a star.

Cortical Myelin Reductions Revealed Cortical Depth-Dependent Profiles

During motor movements, area 3b receives tactile input from the thalamus at the cortical layer IV, whereas area 4 receives motor commands at somewhat more superficial cortical layers. We expected cortical myelin reductions at the hand-face border to be situated in middle cortical layers in area 3b and in somewhat more superficial layers in area 4 if myelin reductions were specific with respect to input structures. With respect to output structures, area 4 sends motor output to the corticospinal tract via cortical layer V, whereas area 3b sends sensory output to neighboring cortical areas mainly via superficial

layers. Cortical myelin reductions at the hand-face border were hence expected to be situated in superficial cortical layers in area 3b, and in deep cortical layers in area 4, if myelin reductions were specific with respect to output structures.

To investigate this, we conducted ANOVAs with the factors location (hand, hand–face border, and face) and layer (deep, inner middle, outer middle, and superficial). An anatomically motivated layering model was used to define cortical layers (Waehnert et al. 2014). We found a main effect of location ($F_{(2, 12)} = 4.29$ and $P = 0.039$), a main effect of layer ($F_{(3, 18)} = 70.20$ and $P < 10^{-6}$), and an interaction between layer and location within area 4 ($F_{(6, 36)} = 3.31$ and $P = 0.01$), and a main effect of layer within area 3b ($F_{(3, 18)} = 135.96$ and $P < 10^{-6}$). To
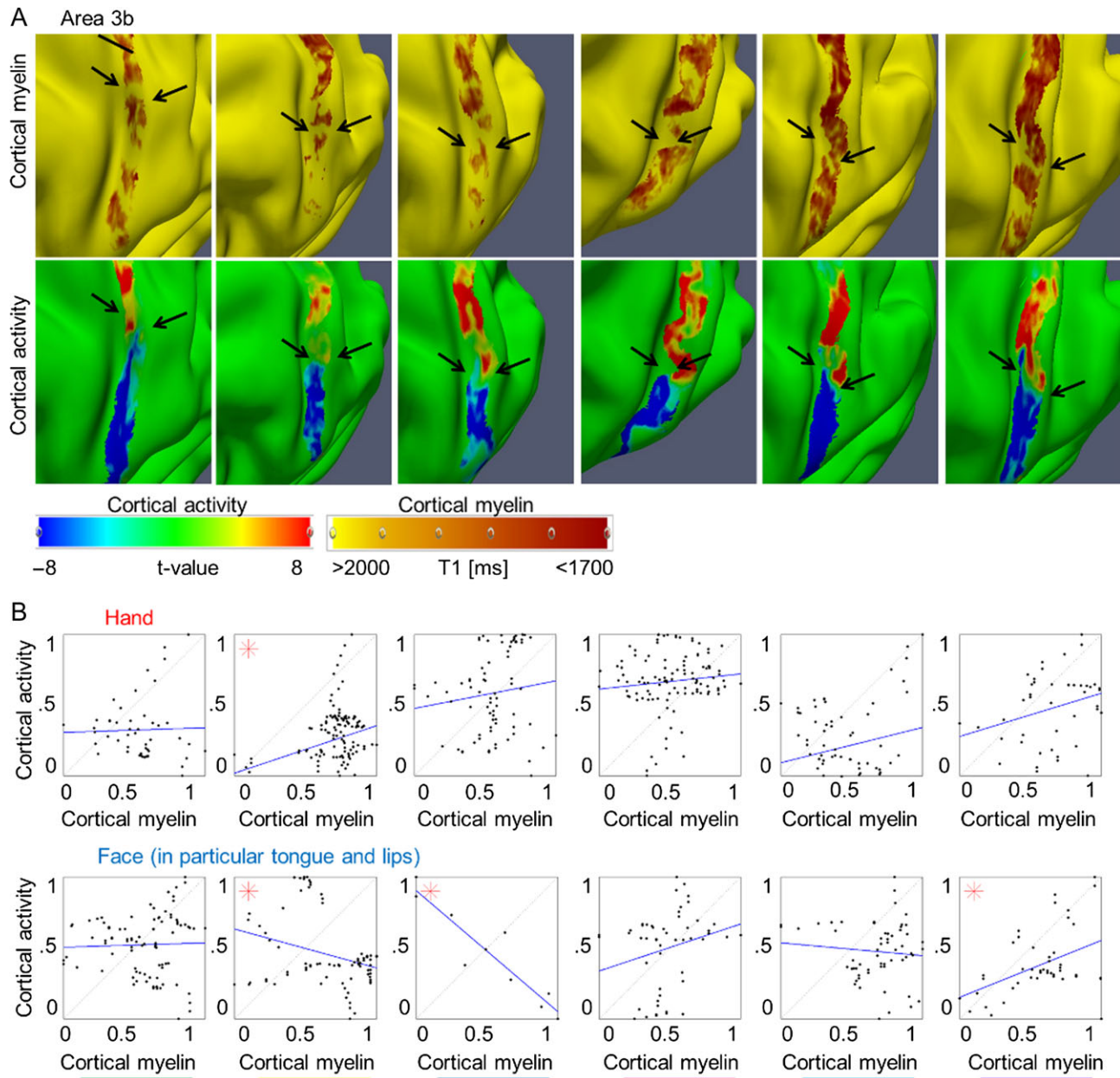
Figure 3. Relationship between cortical myelination and cortical task activation in primary somatosensory cortex: (A) Cortical myelin content (T_1 [ms]) and BOLD signal change (t-values) within primary somatosensory cortex elicited by hand and face (in particular tongue and lip) movements, respectively, of 6 individual participants (see Fig. 2 for remaining participant and see Supplementary Fig. 4 for area 4). The contrast hand − (face + foot) is displayed in red color, the contrast face − (hand + foot) is displayed in blue color. Structural and functional data are masked with the probabilistic FreeSurfer label of area 3b. Arrows indicate the hand–face border, and are placed at corresponding locations within functional and structural images. Cortical myelin content was sampled at 50% cortical depth, because the correspondence between the cortical myelination and the functional hand–face border was most evident in middle cortical layers of area 3b (see Fig. 4). Two millimeter tangential smoothing (i.e., smoothing within cortical layers) was applied to T_1 values for visualization purposes only. (B) Correlations between cortical myelin content (T_1 values, normalized to [0 1] and inverted to correspond to high myelin) and BOLD signal change (t-values, normalized) sampled vertically from hand to face representations (see Supplementary Fig. 6 for sampling paths) within area 3b. Significant correlations (P < 0.0125) are marked with a star. One column represents data of one participant; see Supplementary Figure 3E for color coding.

investigate the significant interaction between location and layer in area 4, we compared cortical myelin values between the centers of the hand and face representation areas with those sampled within the functionally defined hand–face border at different cortical depths (path length = 33.95 mm ± 12.45 mm [mean ± SD]). We found a significant reduction of cortical myelin (corresponding to an increase in T_1 values) between the functionally defined hand representation and the functionally defined

hand–face border in superficial and inner middle layers of area 4 (P < 0.05, see Fig. 4B,C and Table 2). In an exploratory analysis, we also investigated whether significant myelin reductions were confined to specific layers within area 3b (path length area 3b = 32.85 mm ± 11.83 mm, see Supplementary Fig. 6C for path visualizations). We found a significant reduction of cortical myelin (corresponding to an increase in T_1 values) between the functionally defined hand representation and the functionally defined
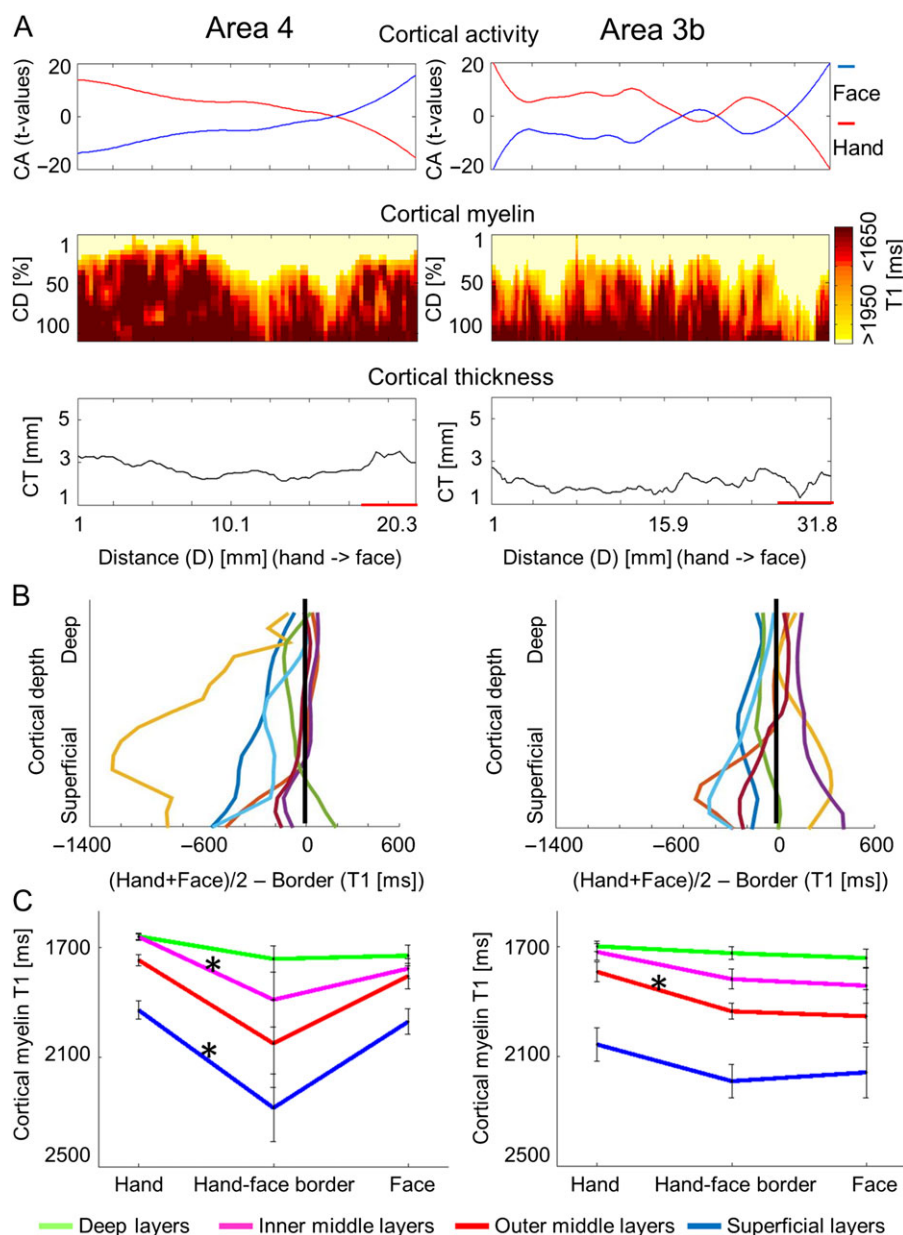
Figure 4. Cortical depth-dependent reduction of cortical myelination between hand and face representation areas using quantitative imaging. (A) Cortical activation (CA, t-values, upper panel), cortical depth-dependent myelination (CD, T_1 [ms], middle panel), and CT ([mm], lower panel) sampled along cortical paths running from functionally defined hand representations to functionally defined face representations (D is the distance on cortical surface, see Supplementary Fig. 6 for sampling paths). Data are shown for primary somatosensory cortex (area 3b) and primary motor cortex (area 4). (B) Cortical depth-dependent myelin reductions between body part representations and hand–face border corrected for the global decrease of cortical myelination in inferior areas. Each line represents one participant. (C) Group-averaged ($N = 7$) cortical myelination (T_1 [ms]) sampled from functionally defined hand representations, functionally defined hand–face borders, and functionally defined face representations (mean ± SEM). Different colors indicate different cortical depths. Each color represents averaged data of 4 modeled cortical layers. Significant comparisons ($P < 0.05$) are marked with a star. Note that higher T_1 values reflect lower cortical myelin.

hand–face border in outer middle layers of area 3b ($P < 0.05$, see Fig. 4C and Table 2).

Cortical myelination often covaries with CT (Sereno et al. 1995). To see whether this was the case at the hand–face border, we compared CT values between our sample points using a Bonferroni-corrected significance threshold of $P < 0.0125$ (4 comparisons, two in each area). We found no significant differences in CT in area 3b (CT hand representation = 2.11 mm ± 0.40 mm [mean ± SD], CT hand–face border = 2.15 mm ± 0.53 mm, CT face representation = 2.21 mm ± 0.27 mm, both $P > 0.8$), and area 4 (CT hand representation = 3.15 mm ± 0.42 mm; CT hand–face

border = 3.81 mm ± 2.22 mm, $P > 0.4$; CT face representation = 4.39 mm ± 2.28 mm; CT hand–face border = 3.81 mm ± 2.22 mm, $P > 0.02$; see Fig. 4A and Supplementary Fig. 6A,B).

Cortical Myelin Borders (Minima) Correspond to Shifts in Pattern of Intrinsic Functional Connectivity

The correlation of intrinsic fluctuations in fMRI signal reflects the spatial organization of functional networks (Biswal et al. 1995; Smith et al. 2009). To assess whether topographic parcellation reflects functional network structure, we compared the

Table 2. Cortical depth-dependent reduction of cortical myelin between hand and face (in particular lower face, lip, tongue) representations using defined paths based on individual cortical folding patterns

Layer	Primary motor cortex					Primary somatosensory cortex				
	Hand		Border		Face	Hand		Border		Face
1 (D)	1640.8 ± 10.9		1679.2 ± 25.6		1691.1 ± 24.6	1676.1 ± 17.9		1680.8 ± 25.5		1705.3 ± 30.3
		$P = 0.24$		$P = 0.70$			$P = 0.90$		$P = 0.63$	
2 (D)	1662.4 ± 13.4		1721.6 ± 36.7		1701.7 ± 30.1	1697.2 ± 19.4		1708.5 ± 23.3		1728.9 ± 31.7
		$P = 0.18$		$P = 0.72$			$P = 0.76$		$P = 0.65$	
3 (D)	1670.6 ± 15.6		1756.3 ± 46.7		1773.8 ± 62.4	1711.8 ± 21.2		1740.0 ± 24.2		1755.2 ± 35.0
		$P = 0.13$		$P = 0.74$			$P = 0.47$		$P = 0.72$	
4 (D)	1669.9 ± 16.1		1815.0 ± 82.6		1758.7 ± 47.2	1715.4 ± 22.9		1770.6 ± 27.4		1781.4 ± 40.5
		$P = 0.12$		$P = 0.46$			$P = 0.22$		$P = 0.81$	
5 (IM)	1663.9 ± 14.3		1848.4 ± 94.3		1778.0 ± 52.2	1716.1 ± 25.9		1794.2 ± 31.6		1804.0 ± 47.6
		$P = 0.08$		$P = 0.38$			$P = 0.12$		$P = 0.85$	
6 (IM)	1657.1 ± 13.2		1869.3 ± 90.45		1762.2 ± 32.9	1718.1 ± 29.5		1812.4 ± 35.4		1829.8 ± 58.8
		$P = 0.04^*$		$P = 0.31$			$P = 0.08$		$P = 0.78$	
7 (IM)	1658.7 ± 11.8		1904.8 ± 100.4		1790.0 ± 36.3	1722.1 ± 33.1		1827.0 ± 39.4		1857.2 ± 71.0
		$P = 0.03^*$		$P = 0.29$			$P = 0.08$		$P = 0.68$	
8 (IM)	1672.2 ± 11.8		1944.5 ± 119.2		1782.9 ± 37.3	1725.9 ± 36.3		1844.8 ± 41.0		1883.4 ± 81.7
		$P = 0.04^*$		$P = 0.28$			$P = 0.07$		$P = 0.67$	
9 (OM)	1697.7 ± 12.9		1990.3 ± 143.3		1785.9 ± 43.7	1737.9 ± 37.4		1872.3 ± 37.1		1907.6 ± 89.9
		$P = 0.07$		$P = 0.26$			**$P = 0.05^*$**		$P = 0.72$	
10 (OM)	1729.7 ± 16.6		2029.7 ± 157.9		1798.1 ± 49.8	1769.4 ± 35.7		1908.4 ± 29.3		1937.6 ± 94.4
		$P = 0.09$		$P = 0.25$			**$P = 0.04^*$**		$P = 0.79$	
11 (OM)	1762.0 ± 23.9		2068.7 ± 165.7		1810.0 ± 51.5	1808.7 ± 37.7		1955.1 ± 31.2		1969.8 ± 99.7
		$P = 0.09$		$P = 0.22$			**$P = 0.05^*$**		$P = 0.91$	
12 (OM)	1801.1 ± 28.2		2116.9 ± 170.9		1829.8 ± 43.4	1856.3 ± 42.9		2012.3 ± 45.5		2005.1 ± 102.7
		$P = 0.09$		$P = 0.16$			$P = 0.08$		$P = 0.96$	
13 (S)	1840.4 ± 32.1		2157.0 ± 145.5		1875.8 ± 41.0	1917.4 ± 50.7		2081.8 ± 63.8		2051.8 ± 101.3
		$P = 0.05^*$		$P = 0.11$			$P = 0.13$		$P = 0.85$	
14 (S)	18823.3 ± 33.9		2217.2 ± 116.9		1942.8 ± 51.2	1996.9 ± 59.4		2150.1 ± 71.4		2106.3 ± 97.1
		$P = 0.02^*$		$P = 0.07$			$P = 0.20$		$P = 0.80$	
15 (S)	1941.9 ± 36.2		2318.3 ± 117.2		1988.3 ± 48.4	2098.2 ± 64.7		2221.7 ± 66.0		2185.6 ± 94.7
		$P = 0.02^*$		**$P = 0.04^*$**			$P = 0.29$		$P = 0.82$	
16 (S)	2055.2 ± 44.8		2451.7 ± 127.6		2080.6 ± 57.1	2219.0 ± 67.9		2312.2 ± 60.1		2294.4 ± 93.3
		$P = 0.04^*$		**$P = 0.04^*$**			$P = 0.40$		$P = 0.89$	

Notes: T_1 values (ms) extracted from different cortical depths and brain areas (primary motor cortex and primary somatosensory cortex) are shown as mean ± SEM. Values were extracted from functionally defined hand representations, functionally defined face representations, and the hand–face intersection point (averaged over N = 7 participants). Note that high values correspond to low cortical myelin. Significant comparisons ($P < 0.05$) are marked with a star and are printed in bold. D, deep cortical layers; IM, inner middle cortical layers; OM, outer middle cortical layers; S, superficial cortical layers.

functional connectivity of each pair of vertices along the previously described paths running parallel to the central sulcus (see Fig. 5; Supplementary Figs 7 and 2A for path visualization). While local functional connectivity to proximate vertices was consistently highest, correlations were also higher within the same topographic area (Chen et al. 2011; Long et al. 2014), with the primary division coinciding with the within-3b and within-4 cortical myelin borders (see Fig. 5 and Supplementary Fig. 7). The identified area of reduced myelination had particularly lower local connectivity, as assessed by calculating the mean correlation of each node to its neighbors within a 4 mm radius along the predefined paths (see Supplementary Fig. 7). Notably, when sampling intrinsic functional connectivity values (*r*) along the cortical paths, we observed higher functional connectivity between hand representations of area 3b and area 4, and face representations of area 3b and area 4, compared with hand and face correlations within each nominal cortical area (see Fig. 5).

Discussion

Our findings demonstrate that human area 3b and area 4 are not homogenous, but are subdivided into distinct cortical fields,

each representing a major body part. Myelin borders coincide with intrinsic functional connectivity borders as measured during the resting state, and show layer-specific reductions within area 3b and area 4. Our data point to a topographic parcellation model of human sensorimotor cortex and suggest that body parts may be an important organizing principle, similar to sensory and motor processing. This has implications for models of the structure, connectivity, function, and plasticity of the sensorimotor system, as discussed below.

Our data suggest modification of current brain atlases that depict area 3b and area 4 as homogenous areas. Also several other research teams recently proposed reconsideration of Brodmann's original map (Amunts and Zilles 2015; Wang et al. 2015; Glasser et al. 2016). For example, Brodmann classified visual area 19 as homogenous. However, the cortical territory spanning area 19 is structurally inhomogeneous (Sereno et al. 2013) and turned out to contain multiple retinotopic maps (Sereno et al. 1995; Angelucci et al. 2015), and multiple cortical fields, including, for example, area MT/V5. Similarly, by combining in vivo cortical myeloarchitecture with topographic maps and functional connectivity analyses, Glasser et al. (2016) identified multiple novel areas in Brodmann area 6, including
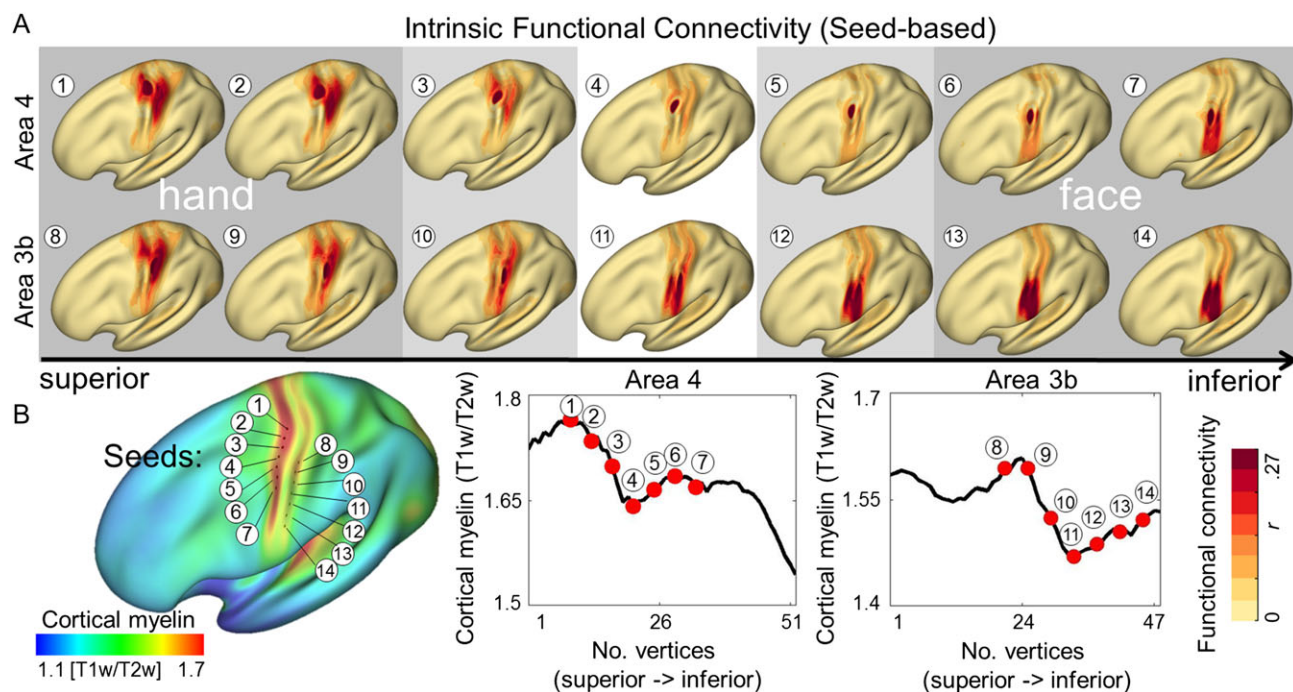
Figure 5. Relationship between cortical myelination and whole-brain intrinsic functional connectivity networks. (A) Intrinsic functional connectivity (seed-based) of averaged group images (HCP). Seeds were placed within primary somatosensory cortex (area 3b) and primary motor cortex (area 4). Numbers correspond to vertex locations as displayed in (B). (B) Cortical myelination (T1w/T2w) displayed on an averaged group image. Seeds were placed at every fourth vertex starting from the vertex with the global myelin minimum. Seed locations are marked as black dots on inflated surface.

area 6mp, 6ma, and the SCEF. Our study suggests that parcellation atlases will benefit by explicitly combining functional imaging with quantitative cytoarchitectonic and myeloarchitectonic mapping techniques in the same set of subjects (Amunts and Zilles 2015; Glasser et al. 2016).

A critical question emerges: Are hand and face representations in area 3b and area 4 (meso-maps), or should they be classified as micromaps, nonrepetitive elements that occur within a given area (Amunts and Zilles 2015)? Cortical structures can be as assigned meso-maps, if they have specific functions in terms of cognitive or mental processes, specific connectivity patterns, offer reproducibility, multimodality, evolutionary coherence, and generalization from one brain to another (Amunts and Zilles 2015). Former experiments have assigned specific functions to somatotopic processing in humans, not only in terms of selective activation during motor movements or sensory perception (Penfield and Boldrey 1937), but also during cognitive tasks, such as during language processing (Kuipers et al. 2013; Mollo et al. 2016), arithmetic (Harvey et al. 2013), working memory (Kastner et al. 2007; Barsalou 2008), and visual perception (Orlov et al. 2010). Somatotopy serves as an organizing element from subcortical structures up to the highest-level cortical areas (Brooks et al. 2005; Sereno and Huang 2006; Nanbu 2009; Orlov et al. 2010; Pereira et al. 2013; Rech et al. 2015; Zeharia et al. 2015). In addition, functional connectivity is altered at the structural hand–face border, both using local and global metrics. Our definition of the hand–face border was automated, reproducible, relied on statistical metrics, and the border could be identified with different structural markers (i.e., quantitative T_1, T1w/T2w-ratio, and T2*). Similar structures exist in nearly related primates (see below), and because of different developmental phases of extremities and head nerves, sensory and motor nerves of the same body part representation across the sensorimotor border may be phylogenetically closer than sensory and

motor nerves within sensory or motor cortex (Flechsig 1920). The classification of hand and face areas as meso-maps would be in accordance with the atlases as proposed by Flechsig (1920) and von Economo and Koskinas (1925), but is in disagreement with the Brodmann atlas (Brodmann 1909). More analyses, in particular those including genetic markers, structural connectivity, and postmortem data are needed for final clarification.

Our findings imply that body parts may be an important organizing principle, similar to the distinction between sensory and motor processing. Besides myeloarchitecture (Flechsig 1920), cytoarchitectonic features within area 3b and area 4 are also not homogenous (von Economo and Koskinas 1925). In fact, it is possible that hand and face areas may actually have mosaic origins (Flechsig 1920). This would be similar to birds, where wing and neck representations are located in distant and separate telencephalic fields (Funke 1989). Reducing the thickness of myelin sheaths, which reduces the frequency and speed of neuronal signal flow along axons (Pajevic et al. 2014; Grydeland et al. 2015), may be a particularly efficient way to enforce modality-specific body part separation and functional specialization. Decreased cell density, which, similar to the reduced thickness of myelin sheaths also causes an increase of the T_1 signal, may limit the amount and complexity of information conveyed across the hand–face border (Collins et al. 2010). The structural separation of body parts within the same modality may allow the development of specialized skills, both ontogenetically and phylogenetically, such as flying and singing in birds, or tool use and language production in humans.

This provides a new perspective on the architecture of the sensorimotor system. For example, it is often assumed that humans are uniquely flexible in adapting topographic maps based on environmental influences in early development, in the course of learning, after cortical or peripheral damage, or with advancing age (Cohen et al. 1993; Agliotti, Bonazzi, et al. 1994,

Aglioti, Cortese, et al.1994; Borsook et al. 1998; Calford 2002; Pleger et al. 2003; Cooke and Bliss 2006; Bedny et al. 2015). However, this has most often been conceptualized as a process that takes place within the boundaries of area 3b and/or area 4. Instead, our data indicate that human topographic maps in sensory and motor cortices have internal boundaries that may limit plasticity in much the same way that we imagine plastic change being limited by boundaries between nominal cortical areas. This may have implications for therapeutic interventions in the sensorimotor domain, such as those applied after stroke, after central damage, in the elderly (Dinse et al. 2006), after limb amputation (Makin et al. 2013), or in people with spinal cord injury (Jain et al. 1997; Saadon-Grosman et al. 2015), where cortical map architecture relates to symptom severity.

Our data question the widespread concept of a "soft-wired brain." The degree to which cortical myelin boundaries in the animal brain limit plastic reorganization in the cortex has been a subject of debate (Jain et al. 1997, 1998, 2001; Sereno 2005). However, a recent definitive study showed that in monkeys with chronic lesions of the dorsal column of spinal cord that had resulted in large-scale map reorganization of hand and face representations in area 3b, nevertheless showed a striking absence of new intracortical projections across the hand–face border (Chand and Jain 2015). Even if few novel connections may appear (Liao et al. 2016), this indicates that map reorganization may be driven more by changes at subcortical (or higher cortical) levels, and that cortical boundaries between major body part representations may limit plastic reorganization at the level of the primary sensorimotor cortex. Our data provide evidence for a similar anatomical substrate in the human brain, which may explain recent observations of preserved topographic map architecture in sensorimotor cortex after sensory loss due to amputation (Makin et al. 2013, 2015; Kikkert et al. 2016).

Our investigation has shown complex relationships between cortical layer-specific myelination, functional topographic maps, and resting state signal fluctuations in the living, human individual. Area 3b as a sensory input area receives its main input from the thalamus in cortical layer IV, whereas area 4 as a motor output area receives input in somewhat more superficial cortical layers. Cortical myelin reductions at the hand–face border were significant in middle cortical layers in area 3b, and in more superficial cortical layers in area 4. Note that whereas the area by layer interaction was significant in area 4, it was not significant in area 3b, which makes the results of area 3b more exploratory. Our data, however, give a first indication that cortical layer-specific myelin reductions may respect input structures in area 3b and area 4. Output structures, on the other hand, were only captured by area 4, as evidenced by the significant reduction of cortical myelin in its deep cortical layers, perhaps encompassing the output layer V. This may indicate segregated signal input in area 3b with reduced feedforward specificity toward its output layers. The high evolutionary pressure on motor output specificity, that is, to clearly control hand and face movements, might have resulted in myelin reductions in area 4 input and output layers to aid separation. If confirmed by future studies (note that we had a relatively low number of participants for the layer-dependent analyses, $n = 7$), cortical layer-specific myelin reductions may provide a novel structural marker for fine-grained neuronal signal differentiation within early sensory and motor cortices.

Cortical zones of reduced myelin between adjacent body part representations have been identified in the rodent and monkey sensorimotor cortex. Here, these zones are called septa

(Woolsey and Van der Loos 1970; Welker and Woolsey 1974; Welker 1976; Land and Simons 1985; Furuta et al. 2009). In the well-described "barrel cortical field," area 3b septa, located in the input layer IV, divide the representations of single whiskers on the rodent's face (Welker 1976; Simons 1978). Septa also exist between other body part representations, such as the hand and face (Welker 1976; Fang et al. 2002), different parts of the face (Welker 1976; Jain et al. 2001), and—in the monkey—between single finger representations (Jain et al. 1998; Qi and Kaas 2004). Septa demonstrate reduced lateral neuronal connections to nearby parts of the cortex (Chapin et al. 1987; Hoeflinger et al. 1995; Kim and Ebner 1999; Fang et al. 2002) and often mark sharp functional borders between adjacent body part representations (Welker 1976; Chapin and Lin 1984). The structures we identified here offer striking similarities to septa as identified in animal brains. Whether borders of reduced cortical myelin also separate other body part representations in humans, as in monkeys and rodents, remains to be clarified. Our data indicate further structural borders within the hand representation of area 3b and superior to the representation of the hand in area 4 (see Fig. 1). Glasser et al. (2016) provide evidence that also eyes, trunk, and lower limb representations may contain distinct structural and functional features. However, the authors assigned these representations the status of a subarea (Glasser et al. 2016).

T_1-based image contrast was used here to map cortical myelin in vivo. But how valid is this measure? A recent study showed that cortical myelination contributes about 64% to quantitative T_1 image contrast, whereas the contribution of iron is about 30% (Stüber et al. 2014). T_1 mapping is also largely unaffected by the direction of myelinated fibers (Stüber et al. 2014), and interregional variation in manganese concentration does not parallel the interregional variation of T_1 values in human cortex (Gelman et al. 2001). Though there are other influences on T_1 contrast, cortical myelin is likely the major underlying contribution to the microstructural differences illustrated here. Definite answers, however, regarding the neuronal structures underlying the observed in vivo effects can only be provided by postmortem descriptions of cortical myelo- and/or cytoarchitecture (Flechsig 1920; von Economo and Koskinas 1925), ideally combined with MR imaging (Caspers et al. 2006), and detailed maps of receptor architectures (Caspers et al. 2015). In addition, diffusion-weighted imaging at ultra-high field may be used to differentiate T_1 signal change driven by axonal diameter and axonal density (De Santis et al. 2016).

Area 3a, which resides deep within the central sulcus and mainly receives input from proprioceptors, separates area 4 from area 3b. Area 3a was not investigated here, which will be required to generalize our findings across the sensorimotor domain. It is also worth mentioning that our study did not allow a specific skin-surface localization of the detected structural border. Future studies should delineate whether the detected border separates the thumb from the lower face, as we assume, or the thumb and lower face from the lip (Manger et al. 1997). Whole-body mapping techniques will be crucial for further addressing this aspect of cortical topography (Zeharia et al. 2015; Sood and Sereno 2016).

Our data suggest that human primary somatosensory cortex and primary motor cortex should no longer be regarded as homogenous areas. Instead, they appear to be subdivided into distinct cortical fields, each representing a major body part, and separated by borders of reduced cortical myelin. This confirms early speculations by Flechsig (1920) about a topographic parcellation scheme in humans, and is in line with

recent evidence suggesting other subdivisions and parcellations of Brodmann's original map (Amunts and Zilles 2015; Glasser et al. 2016). The findings here offer new mechanistic insights into sensory and motor cortical functions in health and disease.

Supplementary Material

Funding

Notes

Conflict of Interest: None declared.

References

Aglioti S, Bonazzi A, Cortese F. 1994. Phantom lower limb as a perceptual marker of neural plasticity in the mature human brain. Proc Biol Sci. 255:273–278.

Aglioti S, Cortese F, Franchini C. 1994. Rapid sensory remapping in the adult human brain as inferred from phantom breast perception. Neuroreport. 5:473–476.

Amunts K, Zilles K. 2015. Architectonic mapping of the human brain beyond Brodmann. Neuron. 88:1086–1107.

Angelucci AR, Roe AW, Sereno MI. 2015. Controversial issues in visual cortex mapping: extrastriate cortex between areas V2 and MT in human and nonhuman primates. Visual Neurosci. 32:E025.

Avants BB, Epstein CL, Grossman M, Gee JC. 2008. Symmetric diffeomorphic image registration with cross-correlation: evaluating automated labeling of elderly and neurodegenerative brain. Med Image Anal. 12:26–41.

Barsalou LW. 2008. Grounded cognition. Annu Rev Psychol. 59: 617–645.

Bazin PL, Weiss M, Dinse J, Schäfer A, Trampel R, Turner R. 2014. A computational framework for ultra-high resolution cortical segmentation at 7 Tesla. Neuroimage. 93 (Pt 2):201–209.

Beckmann CF, Smith SM. 2004. Probabilistic independent component analysis for functional magnetic resonance imaging. IEEE Trans Med Imaging. 23:137–152.

Bedny M, Richardson H, Saxe R. 2015. "Visual" cortex responds to spoken language in blind children. J Neurosci. 35: 11674–11681.

Biswal B, Yetkin FZ, Haughton VM, Hyde JS. 1995. Functional connectivity in the motor cortex of resting human brain using echo-planar MRI. Magn Reson Med. 34:537–541.

Borsook D, Becerra L, Fishman S, Edwards A, Jennings CL, Stojanovic M, Papinicolas L, Ramachandran VS, Gonzalez RG, Breiter H. 1998. Acute plasticity in the human

somatosensory cortex following amputation. Neuroreport. 9:1013–1017.

Brodmann K. 1909. Vergleichende Lokalisationslehre der Grosshirnrinde in ihren Prinzipien dargestellt auf Grund des Zellbaues. Leipzig (Germany): (J.A. Barth).

Brooks JC, Zambreanu L, Godinez A, Craig AD, Tracey I. 2005. Somatotopic organisation of the human insula to painful heat studied with high resolution functional imaging. Neuroimage. 27:201–209.

Calford MB. 2002. Dynamic representational plasticity in sensory cortex. Neuroscience. 111:709–738.

Caspers J, Palomero-Gallagher N, Caspers S, Schleicher A, Amunts K, Zilles K. 2015. Receptor architecture of visual areas in the face and word-form recognition region of the posterior fusiform gyrus. Brain Struct Funct. 220:205–219.

Caspers S, Geyer S, Schleicher A, Mohlberg H, Amunts K, Zilles K. 2006. The human inferior parietal cortex: cytoarchitectonic parcellation and interindividual variability. Neuroimage. 33: 430–448.

Chand P, Jain N. 2015. Intracortical and thalamocortical connections of the hand and face representations in somatosensory area 3b of macaque monkeys and effects of chronic spinal cord injuries. J Neurosci. 35:13475–13486.

Chapin JK, Lin CS. 1984. Mapping the body representation in the SI cortex of anesthetized and awake rats. J Comp Neurol. 229:199–213.

Chapin JK, Sadeq M, Guise JL. 1987. Corticocortical connections within the primary somatosensory cortex of the rat. J Comp Neurol. 263:326–346.

Chen L, Mishra A, Newton AT, Morgan VL, Stringer EA, Rogers BP, Gore JC. 2011. Fine-scale functional connectivity in somatosensory cortex revealed by high-resolution fMRI. Magn Reson Imaging. 29:1330–1337.

Cohen LG, Brasil-Neto JP, Pascual-Leone A, Hallett M. 1993. Plasticity of cortical motor output organization following deafferentation, cerebral lesions, and skill acquisition. Adv Neurol. 63:187–200.

Collins CE, Airey DC, Young NA, Leitch DB, Kaas JH. 2010. Neuron densities vary across and within cortical areas in primates. Proc Natl Acad Sci USA. 107:15927–15932.

Cooke SF, Bliss TV. 2006. Plasticity in the human central nervous system. Brain. 129:1659–1673.

De Santis S, Assaf Y, Jeurissen B, Jones DK, Roebroeck A. 2016. T1 relaxometry of crossing fibres in the human brain. Neuroimage. 141:133–142.

Deistung A, Schafer A, Schweser F, Biedermann U, Turner R, Reichenbach JR. 2013. Toward in vivo histology: a comparison of quantitative susceptibility mapping (QSM) with magnitude-, phase-, and R2*-imaging at ultra-high magnetic field strength. Neuroimage. 65:299–314.

Dick F, Tierney AT, Lutti A, Josephs O, Sereno MI, Weiskopf N. 2012. In vivo functional and myeloarchitectonic mapping of human primary auditory areas. J Neurosci. 32:16095–16105.

Dinse HR, Kleibel N, Kalisch T, Ragert P, Wilimzig C, Tegenthoff M. 2006. Tactile coactivation resets age-related decline of human tactile discrimination. Ann Neurol. 60:88–94.

Dinse J, Härtwich N, Waehnert M, Tardif C, Schäfer A, Geyer S, Preim B, Turner R, Bazin PL. 2015. A cytoarchitecture-driven myelin model reveals area-specific signatures in human primary and secondary areas using ultra-high resolution invivo brain MRI. Neuroimage. 114:71–87.

Fang PC, Jain N, Kaas JH. 2002. Few intrinsic connections cross the hand–face border of area 3b of New World monkeys. J Comp Neurol. 454:310–319.

Flechsig P. 1920. Anatomie des menschlichen Gehirns und Rückenmarks. Leipzig (Germany): Verlag von Georg Thieme.

Funke K. 1989. Somatosensory areas in the telencephalon of the pigeon. I. Response characteristics. Exp Brain Res. 76: 603–619.

Furuta T, Kaneko T, Deschenes M. 2009. Septal neurons in barrel cortex derive their receptive field input from the lemniscal pathway. J Neurosci. 29:4089–4095.

Gelman N, Ewing JR, Gorell JM, Spickler EM, Solomon EG. 2001. Interregional variation of longitudinal relaxation rates in human brain at 3.0 T: relation to estimated iron and water contents. Magn Reson Med. 45:71–79.

Glasser MF, Coalson TS, Robinson EC, Hacker CD, Harwell J, Yacoub E, Ugurbil K, Andersson J, Beckmann CF, Jenkinson M, et al. 2016. A multi-modal parcellation of human cerebral cortex. Nature. 536:171–178.

Glasser MF, Sotiropoulos SN, Wilson JA, Coalson TS, Fischl B, Andersson JL, Xu J, Jbabdi S, Webster M, Polimeni JR, et al. 2013. The minimal preprocessing pipelines for the Human Connectome Project. Neuroimage. 80:105–124.

Glasser MF, Van Essen DC. 2011. Mapping human cortical areas in vivo based on myelin content as revealed by T1- and T2-weighted MRI. J Neurosci. 31:11597–11616.

Glover GH. 1999. Deconvolution of impulse response in event-related BOLD fMRI. Neuroimage. 9:416–429.

Groppe DM, Urbach TP, Kutas M. 2011a. Mass univariate analysis of event-related brain potentials/fields I: a critical tutorial review. Psychophysiology. 48:1711–1725.

Groppe DM, Urbach TP, Kutas M. 2011b. Mass univariate analysis of event-related brain potentials/fields II: simulation studies. Psychophysiology. 48:1726–1737.

Grydeland H, Westlye LT, Walhovd KB, Fjell AM. 2015. Intracortical posterior cingulate myelin content relates to error processing: results from T1- and T2-weighted MRI myelin mapping and electrophysiology in healthy adults. Cereb Cortex. 26:2402–2410.

Han X, Pham DL, Tosun D, Rettmann ME, Xu C, Prince JL. 2004. CRUISE: cortical reconstruction using implicit surface evolution. Neuroimage. 23:997–1012.

Harvey BM, Klein BP, Petridou N, Dumoulin SO. 2013. Topographic representation of numerosity in the human parietal cortex. Science. 341:1123–1126.

Hoeflinger BF, Bennett-Clarke CA, Chiaia NL, Killackey HP, Rhoades RW. 1995. Patterning of local intracortical projections within the vibrissae representation of rat primary somatosensory cortex. J Comp Neurol. 354:551–563.

Hopf A. 1969. Photometric studies on the myeloarchitecture of the human parietal lobe. I. Parietal region. J Hirnforsch. 11: 253–265.

Hurley AC, Al-Radaideh A, Bai L, Aickelin U, Coxon R, Glover P, Gowland PA. 2010. Tailored RF pulse for magnetization inversion at ultrahigh field. Magn Reson Med. 63:51–58.

Jain N, Catania KC, Kaas JH. 1997. Deactivation and reactivation of somatosensory cortex after dorsal spinal cord injury. Nature. 386:495–498.

Jain N, Catania KC, Kaas JH. 1998. A histologically visible representation of the fingers and palm in primate area 3b and its immutability following long-term deafferentations. Cereb Cortex. 8:227–236.

Jain N, Qi HX, Catania KC, Kaas JH. 2001. Anatomic correlates of the face and oral cavity representations in the somatosensory cortical area 3b of monkeys. J Comp Neurol. 429:455–468.

Jovicich J, Czanner S, Greve D, Haley E, van der Kouwe A, Gollub R, Kennedy D, Schmitt F, Brown G, Macfall J, et al. 2006. Reliability in multi-site structural MRI studies: effects of gradient non-linearity correction on phantom and human data. Neuroimage. 30:436–443.

Kastner S, DeSimone K, Konen CS, Szczepanski SM, Weiner KS, Schneider KA. 2007. Topographic maps in human frontal cortex revealed in memory-guided saccade and spatial working-memory tasks. J Neurophysiol. 97: 3494–3507.

Kikkert S, Kolasinski J, Jbabdi S, Tracey I, Beckmann CF, Johansen-Berg H, Makin TR. 2016. Revealing the neural fingerprints of a missing hand. Elife. 5: e15292, 1–19.

Kim U, Ebner FF. 1999. Barrels and septa: separate circuits in rat barrels field cortex. J Comp Neurol. 408:489–505.

Kuipers JR, van Koningsbruggen M, Thierry G. 2013. Semantic priming in the motor cortex: evidence from combined repetitive transcranial magnetic stimulation and event-related potential. Neuroreport. 24:646–651.

Land PW, Simons DJ. 1985. Cytochrome oxidase staining in the rat SmI barrel cortex. J Comp Neurol. 238:225–235.

Liao CC, Reed JL, Kaas JH, Qi HX. 2016. Intracortical connections are altered after long-standing deprivation of dorsal column inputs in the hand region of area 3b in squirrel monkeys. J Comp Neurol. 524:1494–1526.

Long X, Goltz D, Margulies DS, Nierhaus T, Villringer A. 2014. Functional connectivity-based parcellation of the human sensorimotor cortex. Eur J Neurosci. 39:1332–1342.

Lucas BC, Bogovic JA, Carass A, Bazin PL, Prince JL, Pham DL, Landman BA. 2010. The Java Image Science Toolkit (JIST) for rapid prototyping and publishing of neuroimaging software. Neuroinformatics. 8:5–17.

Lutti A, Dick F, Sereno MI, Weiskopf N. 2014. Using high-resolution quantitative mapping of R1 as an index of cortical myelination. Neuroimage. 93 (Pt 2):176–188.

Makin TR, Scholz J, Filippini N, Henderson Slater D, Tracey I, Johansen-Berg H. 2013. Phantom pain is associated with preserved structure and function in the former hand area. Nat Comm. 4:1570.

Makin TR, Scholz J, Henderson Slater D, Johansen-Berg H, Tracey I. 2015. Reassessing cortical reorganization in the primary sensorimotor cortex following arm amputation. Brain. 138:2140–2146.

Manger PR, Woods TM, Munoz A, Jones EG. 1997. Hand/face border as a limiting boundary in the body representation in monkey somatosensory cortex. J Neurosci. 17: 6338–6351.

Marques JP, Kober T, Krueger G, van der Zwaag W, Van de Moortele PF, Gruetter R. 2010. MP2RAGE, a self bias-field corrected sequence for improved segmentation and T1-mapping at high field. Neuroimage. 49:1271–1281.

McAuliffe MJ, Lalonde FM, McGarry D, Gandler W, Csaky K, Trus BL. 2001. Medical image processing, analysis & visualization in clinical research. Proceedings 14th IEEE Symposium on Computer-Based Medical Systems. CBMS 2001. Bethesda (MD): IEEE. pp. 381–386.

Mitchell JSB, Mount DM, Papadimitrious H. 1987. The discrete geodesic problem. Siam J Comput. 16:21.

Mollo G, Pulvermuller F, Hauk O. 2016. Movement priming of EEG/MEG brain responses for action-words characterizes the link between language and action. Cortex. 74:262–276.

Nakamura A, Yamada T, Goto A, Kato T, Ito K, Abe Y, Kachi T, Kakigi R. 1998. Somatosensory homunculus as drawn by MEG. Neuroimage. 7:377–386.

Nanbu A. 2009. Somatotopy in the basal ganglia. Brain Nerve. 61:1383–1394.

Nieuwenhuys R. 2013. The myeloarchitectonic studies on the human cerebral cortex of the Vogt-Vogt school, and their significance for the interpretation of functional neuroimaging data. Brain Struct Funct. 218:303–352.

Orlov T, Makin TR, Zohary E. 2010. Topographic representation of the human body in the occipitotemporal cortex. Neuron. 68:586–600.

Pajevic S, Basser PJ, Fields RD. 2014. Role of myelin plasticity in oscillations and synchrony of neuronal activity. Neuroscience. 276:135–147.

Penfield W, Boldrey E. 1937. Somatic motor and sensory representation in the cerebral cortex of man as studied by electrical stimulation. Brain. 60:389–443.

Pereira EA, Wang S, Owen SL, Aziz TZ, Green AL. 2013. Human periventricular grey somatosensory evoked potentials suggest rostrocaudally inverted somatotopy. Stereotact Funct Neurosurg. 91:290–297.

Pleger B, Schwenkreis P, Dinse HR, Ragert P, Hoffken O, Malin JP, Tegenthoff M. 2003. Pharmacological suppression of plastic changes in human primary somatosensory cortex after motor learning. Exp Brain Res. 148:525–532.

Qi HX, Kaas JH. 2004. Myelin stains reveal an anatomical framework for the representation of the digits in somatosensory area 3b of macaque monkeys. J Comp Neurol. 477:172–187.

Rech F, Herbet G, Moritz-Gasser S, Duffau H. 2015. Somatotopic organization of the white matter tracts underpinning motor control in humans: an electrical stimulation study. Brain Struct Funct. 221:3743–3753.

Robinson EC, Jbabdi S, Glasser MF, Andersson J, Burgess GC, Harms MP, Smith SM, Van Essen DC, Jenkinson M. 2014. MSM: a new flexible framework for Multimodal Surface Matching. Neuroimage. 100:414–426.

Saadon-Grosman N, Tal Z, Itshayek E, Amedi A, Arzy S. 2015. Discontinuity of cortical gradients reflects sensory impairment. Proc Natl Acad Sci USA. 112:16024–16029.

Sereno MI. 2005. Neuroscience: plasticity and its limits. Nature. 435:288–289.

Sereno MI, Dale AM, Reppas JB, Kwong KK, Belliveau JW, Brady TJ, Rosen BR, Tootell RB. 1995. Borders of multiple visual areas in humans revealed by functional magnetic resonance imaging. Science. 268:889–893.

Sereno MI, Huang RS. 2006. A human parietal face area contains aligned head-centered visual and tactile maps. Nat Neurosci. 9:1337–1343.

Sereno MI, Lutti A, Weiskopf N, Dick F. 2013. Mapping the human cortical surface by combining quantitative T(1) with retinotopy. Cereb Cortex. 23:2261–2268.

Sethian JA. 1999. *Level* set methods and fast marching methods: evolving interfaces in computational geometry, fluid mechanics, computer vision, and materials science. Cambridge (UK): Cambridge University Press.

Simons DJ. 1978. Response properties of vibrissa units in rat SI somatosensory neocortex. J Neurophysiol. 41:798–820.

Smith AC, Monaghan P, Huettig F. 2013. An amodal shared resource model of language-mediated visual attention. Front Psychol. 4:528.

Smith SM, Beckmann CF, Andersson J, Auerbach EJ, Bijsterbosch J, Douaud G, Duff E, Feinberg DA, Griffanti L, Harms MP, et al. 2013. Resting-state fMRI in the Human Connectome Project. Neuroimage. 80:144–168.

Smith SM, Fox PT, Miller KL, Glahn DC, Fox PM, Mackay CE, Filippini N, Watkins KE, Toro R, Laird AR, et al. 2009. Correspondence of the brain's functional architecture during activation and rest. Proc Natl Acad Sci USA. 106:13040–13045.

Sood MR, Sereno MI. 2016. Areas activated during naturalistic reading comprehension overlap topological visual, auditory, and somatotomotor maps. Hum Brain Mapp. 37:2784–2810.

Stüber C, Morawski M, Schäfer A, Labadie C, Waehnert M, Leuze C, Streicher M, Barapatre N, Reimann K, Geyer S, et al. 2014. Myelin and iron concentration in the human brain: a quantitative study of MRI contrast. Neuroimage. 93 (Pt 1):95–106.

Tardif CL, Schafer A, Trampel R, Villringer A, Turner R, Bazin PL. 2016. Open Science CBS Neuroimaging Repository: sharing ultra-high-field MR images of the brain. Neuroimage. 124:1143–1148.

Tardif CL, Schäfer A, Waehnert M, Dinse J, Turner R, Bazin PL. 2015. Multi-contrast multi-scale surface registration for improved alignment of cortical areas. Neuroimage. 111:107–122.

Tosun D, Rettmann ME, Prince JL. 2004. Mapping techniques for aligning sulci across multiple brains. Med Image Anal. 8: 295–309.

Van Essen DC, Smith SM, Barch DM, Behrens TE, Yacoub E, Ugurbil K, Consortium WU-MH. 2013. The WU-Minn Human Connectome Project: an overview. Neuroimage. 80:62–79.

von Economo C, Koskinas G. 1925. Die Cytoarchitektonik der Hirnrinde des Erwachsenen Menschen. Vienna (Austria)/ Berlin (Germany): Springer.

Waehnert MD, Dinse J, Schafer A, Geyer S, Bazin PL, Turner R, Tardif CL. 2016. A subject-specific framework for in vivo myeloarchitectonic analysis using high resolution quantitative MRI. Neuroimage. 125:94–107.

Waehnert MD, Dinse J, Weiss M, Streicher MN, Waehnert P, Geyer S, Turner R, Bazin PL. 2014. Anatomically motivated modeling of cortical laminae. Neuroimage. 93 (Pt 2):210–220.

Wang D, Buckner RL, Fox MD, Holt DJ, Holmes AJ, Stoecklein S, Langs G, Pan R, Qian T, Li K, et al. 2015. Parcellating cortical functional networks in individuals. Nat Neurosci. 18: 1853–1860.

Welker C. 1976. Receptive fields of barrels in the somatosensory neocortex of the rat. J Comp Neurol. 166:173–189.

Welker C, Woolsey TA. 1974. Structure of layer IV in the somatosensory neocortex of the rat: description and comparison with the mouse. J Comp Neurol. 158:437–453.

Woolrich MW, Ripley BD, Brady M, Smith SM. 2001. Temporal autocorrelation in univariate linear modeling of FMRI data. Neuroimage. 14:1370–1386.

Woolsey TA, Van der Loos H. 1970. The structural organization of layer IV in the somatosensory region (SI) of mouse cerebral cortex. The description of a cortical field composed of discrete cytoarchitectonic units. Brain Res. 17:205–242.

Yeo BT, Krienen FM, Sepulcre J, Sabuncu MR, Lashkari D, Hollinshead M, Roffman JL, Smoller JW, Zollei L, Polimeni JR, et al. 2011. The organization of the human cerebral cortex estimated by intrinsic functional connectivity. J Neurophysiol. 106:1125–1165.

Zeharia N, Hertz U, Flash T, Amedi A. 2015. New whole-body sensory-motor gradients revealed using phase-locked analysis and verified using multivoxel pattern analysis and functional connectivity. J Neurosci. 35:2845–2859.